J Electroceram (2012) 29:125–132
DOI 10.1007/s10832-012-9753-0

Varistor behavior of Mn doped ZnO ceramics prepared from nanosized precursors

M. Ebrahimizadeh Abrishami · A. Kompany · S. M. Hosseini

Received: 5 October 2011 / Accepted: 25 June 2012 / Published online: 7 July 2012

Abstract Polycrystalline ZnO doped with MnO, from 2 to 15 mol%, was prepared from nanosized precursors. The effect of Mn doping and sintering temperature on phase evolution, microstructure and V-I characteristics were investigated. SEM images showed that the great merit of using nanoparticles is that the samples with high microstructural uniformity and lower grain size can be achieved. Varistor behavior was observed in all specimens, even in the undoped ceramics due to the oxidation process of zinc interstitial defects at grain boundaries. The electric field versus current density (E-J) curves indicated that the breakdown field E_b increased and the nonlinear coefficient α decreased with the increase in doping level. 2 mol% Mn doped ceramic sintered at 1100 °C exhibited the highest nonlinear coefficient, α=40. The stability test under DC stress was performed for the undoped ZnO ceramics. ZnO varistor sintered at 1300 °C showed not only high nonlinearity, but also high stability under DC stress.

Keywords Varistor · ZnO · Mn doping · Nanopowders · Barrier layer model

1 Introduction

Zinc oxide based varistors have been extensively used in electronic circuits as protection devices against transient over voltages due to the nonlinearity of voltage–current (V-I) characteristic. Several authors have suggested the subtle theories on the operation of varistors [1–5]. The varistors are fabricated by a ceramic sintering process that provides a structure made up of conductive grains surrounded by thin insulating barriers. The unusual V-I characteristic of ZnO based varistors are associated with these insulating barriers. A typical ZnO varistor is normally comprised of several dopants or additives [6–10] and the role of each one is now quite well understood [11–15]. Bi_2O_3 provides the medium for liquid phase sintering and improve the stability of V-I characteristic. In varistor added with MnO and CoO, significant increase of nonlinear coefficient was obtained [15, 16]. As for degradation, addition of Sb_2O_3 turned out to be quite efficient, especially in leakage current I_l [17].

In addition to the chemical composition, the non-ohmic behavior of ZnO varistor strongly depends on the microstructural properties of the samples such as grain size, intergranular layer thickness and porosity [18]. S. Li et al. [19] have suggested that for the smaller grain size, higher breakdown field is obtained and reported elsewhere that the dimensional effect originates for the degree of the heterogeneity of grain size distribution and irregularity of grain shape [20]. The microstructure directly affects the properties of the grain boundaries which have the major role in the V-I characteristics. Better nonlinearity is obtained with the high degree of microstructural uniformity both in size and shape of the grains [21]. A theoretical approach suggests that the electrical properties of ZnO based varistors are improved when the depletion layer becomes narrow [22]. This goal is attained by fabricating ZnO varistor ceramic using nanosized precursors [23–25].

In operation, varistors often undergo various stresses that can affect the device performance and lifetime. Electrical properties may be degraded by continuous leakage current and Joule heat and the rate of degradation can be strongly

M. Ebrahimizadeh Abrishami (✉)
Department of Physics, University of Neyshabur,
Neyshabur, Iran
e-mail: ebrahimizadeh@ymail.com

A. Kompany · S. M. Hosseini
Department of Physics (Materials and Electroceramics Laboratory), Ferdowsi University of Mashhad,
Mashhad, Iran

affected by small changes in the composition. Therefore, the electrical stability is a significant component of ZnO based varistors. The nonlinearity and stability of varistors depend on the chemical composition and the processing technique.

In this paper, a new method of fabricating Mn doped ZnO varistors prepared by nano-composites is put forward. Our research focuses on the effect of chemical composition and ceramic processing on the microstructural uniformity and electrical properties of varistors; in order to find out the perfect varistor parameters such as nonlinear coefficient, breakdown field and leakage current.

2 Experimental procedures

Undoped and Mn-doped ZnO nanoparticles with the mean particle size of about 35 nm were prepared by the sol–gel method. The raw materials used for the synthesis of nanoparticles were zinc acetate dehydrate, $Zn(CH_3COO)_2.2H_2O$ (Merck, 99.5 %), manganese acetate tetrahydrate, $Mn(CH_3COO)_2.4H_2O$ (Merck, 99 %), acetic acid (Merck, 99.8 %) and diethanolamine (DEA) (Merck, 98 %). The molar ratios of the dopant agent were 2, 6, 10, 15 mol%. The details of the synthesis process have been given in the previous work [26]. Ring-shaped specimens were manufactured by pressing the nanopowders under a pressure of 225 bars. Sintering was performed at four different temperatures of 1000 °C, 1100 °C, 1200 °C and 1300 °C. The samples were heated up at a constant rate of 3 °C/min up to sintering temperature keeping for 2 h and then cooled down at the rate of 1 °C/min. A careful temperature control was maintained throughout the heating cycle with a micro-processor controlled furnace.

Samples surfaces were polished to a mirror-like one. The polished samples were thermally etched at 1100 °C for 15 min. The surface microstructure was characterized by using scanning electron microscopy (SEM). The average grain size was determined by the linear intercept method. The density of the samples was measured after sintering by Archimedes' method.

In order to form the ohmic contacts, silver paste was coated on both faces of the samples. The V-I characteristic was examined by using a V-I source measure unit. The obtained curves are divided into two significant regions: Ohmic region with very high resistance before the operation voltage and the well known breakdown region. In the breakdown region of the curves, the current density-electric field relation can be expressed by the empirical relation $J=KE^{\alpha}$, where K is a constant and α is the nonlinear coefficient of the varistor. The nonlinear coefficient was deduced by the equation, $\alpha = 1/(\log E_2 - \log E_1)$ where E_1 and E_2 are the electric fields corresponding to 10^{-1}A/cm^2 and 10^{-3} ^{1}A/cm^2. The varistor voltage ($V_{1\ mA}$) was measured at 1 mA/cm^2 and the breakdown field E_b was defined as $V_{1\ mA}/D$, where D is the thickness of the sample.

The stability test for DC accelerate aging stress were carried out under three continuous conditions (first stress: 0.8 $V_{1\ mA}$/90 °C/12 h, second stress: 0.85 $V_{1\ mA}$/120 °C/12 h, third stress: 0.9 $V_{1\ mA}$/150 °C/12 h) and in order to monitor the thermal runaway status, simultaneously the leakage current was recorded during stressing.

3 Results and discussions

Figure 1 shows the precursor size effects on the appearance of the undoped ZnO ceramic. Both samples were fabricated in a same process, except the size of particles used to prepare the ceramics. The samples in Fig. 1(a) and (b) were made up from large and nanoparticles, respectively. As can be seen in this figure, the appearance of the ceramic fabricated from ZnO nanoparticles had two distinguished differences: more shrinkage and changing color to faint yellow after sintering.

Figure 2 shows the density of the ceramics after sintering. The density of undoped ZnO ceramic was in the range of 5.37 to 5.43 g/cm^3. The density exhibited a significant increase with increasing Mn content. Also, the density slightly increased with increasing sintering temperature probably due to pore reduction. The densification that occurs during the sintering process is a main factor in the resistance of degradation together with a leakage current density in the V-I characteristic and stability of the varistor.

Figure 3 shows the SEM images of polished and thermally etched ceramics sintered at 1000 °C. This figure shows that the morphology in the top of some grains presented a hexagonal spiral growth. The completed and uncompleted spiral curves in some of the ZnO grains corresponded to growth of structures during etching process. It is found from this figure that more homogeneous microstructure can be obtained by using nanostructures. Some evidences of pore distribution observed in the undoped and 2 mol% Mn doped ceramic were reduced with increasing Mn amount. The grain boundaries of the undoped

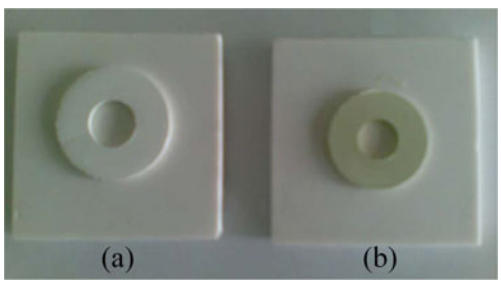

Fig. 1 Photographs of the undoped ZnO ceramics prepared from (**a**) large particles and (**b**) nanoparticles at 1000 °C

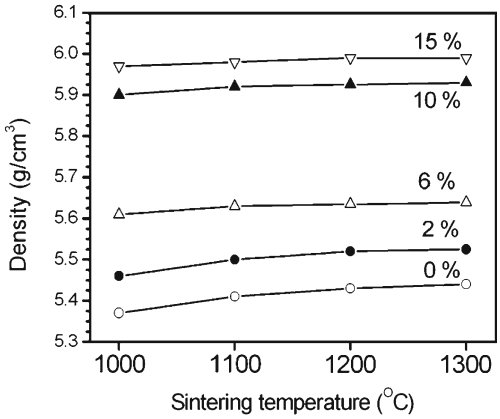

Fig. 2 Density as a function of sintering temperature and MnO content

ceramic were straight while the grain boundaries were curved and numbers of particles were segregated in the heavily doped ceramics due to strong surface tension of Mn compounds at grain boundaries.

A diagram in Fig. 3 presents the changes of average grain size as a function of Mn content for the samples sintered at 1000 °C for 2 h. With the increase in doping level, up to 6 mol% (Figs. 3(a)–(c)), the average grain size slightly increased while with the higher Mn concentration (Figs. 3 (d)–(f)), the average grain size decreased. The average grain size was in the range of 1.2–1.9 μm. The reasons why this technique of fabricating the ZnO based varistors prepared by nanostructures can develop the macroelectrical properties may originate for the improved microstructural uniformity.

Figure 4 shows a typical SEM image of the 2 and 15 mol% Mn doped samples sintered at 1300 °C. Obviously the average grain size increased with the increase of the sintering temperature. Also, Fig. 4(b) indicates that the number of particles in the 15 mol% Mn doped ceramic extremely increased than that of sintered at 1000 °C (Fig. 1(d)).

Figure 5 shows the phase composition of ZnO-MnO (0 and 6 mol%) varistors sintered at 1000 °C. This figure reveals that the grains were mostly crystallized along c-axis and Mn doping did not affect the crystallization orientation. The XRD pattern of 6 mol% Mn doped ceramic indicated that diffraction peaks corresponding to $ZnMn_2O_4$ were observed, confirming the presence of Mn compounds at grain boundaries. The chemical composition of the particles formed at triple points was analyzed by EDX. As shown in the inset of Fig. 5, the major elements at these particles were Zn and Mn.

Figure 6 shows the electric field-current density (E-J) characteristics of the undoped and Mn doped ZnO ceramics sintered at 1000 °C, 1100 °C, 1200 °C and 1300 °C for 2 h. The ceramics are likely to exhibit acceptable varistor characteristic seemingly. The variation of V-I characteristic parameters are summarized in Table 1. One of the most important figures of virtue in varistors is the nonlinear coefficient α. Figure 7 shows the nonlinear coefficient as a function of sintering temperature. The varistor with 2 mol% MnO and sintered at 1100 °C exhibited the highest value α=40 while the higher sintering temperature decreased α. Moreover, increasing doping content further to 2 mol% caused the α value to decrease. Figure 7 gives the relationship between breakdown voltage and the sintering temperature. Despite the grain size of the undoped samples was small, the E_b values were too low (approximately 100 V/cm).

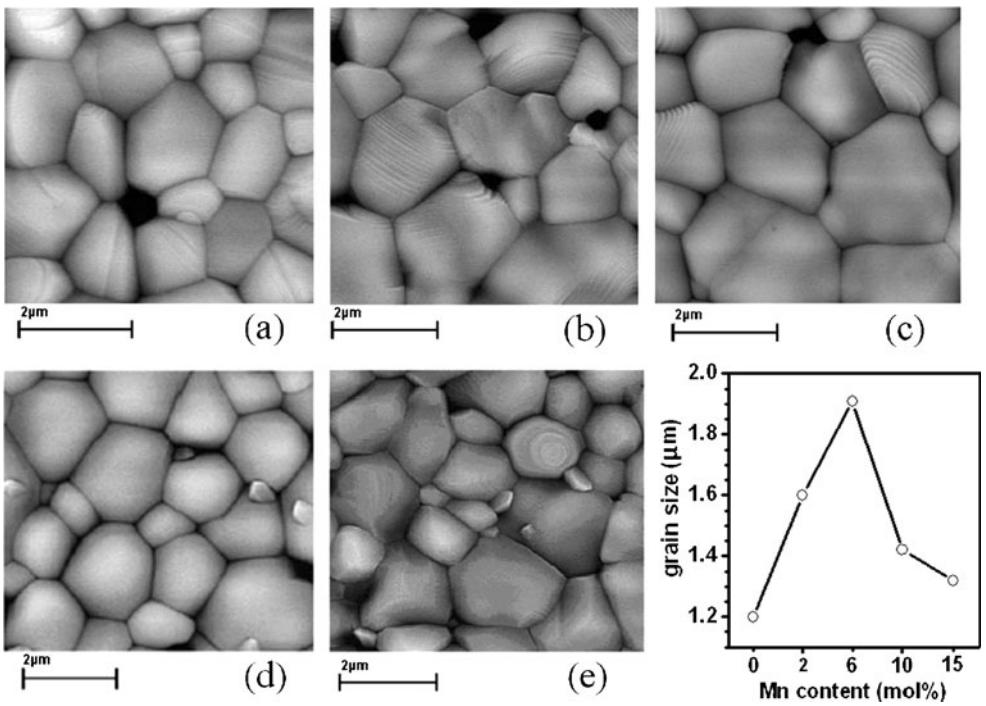

Fig. 3 SEM micrographs of ceramics sintered at 1000 °C for 2 h with various MnO content. (**a**) the undoped ZnO ceramic and (**b**) 2 mol%, (**c**) 6 mol%, (**d**) 10 mol% and (**e**) 15 mol% Mn doped samples

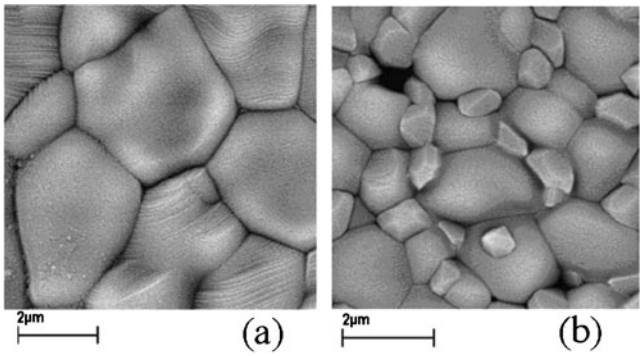

Fig. 4 The typical microstructure of Mn doped ZnO varistors sintered at 1300 °C, (**a**) 2 mol% and (**b**) 15 mol%

In addition to additive effects on varistor properties, sintering temperature affects the microstructure properties such as grain size and depletion layer thickness as well. As shown in Figs. 6(a)–(b), the breakdown region of the samples with 6 and 10 mol% Mn doped samples sintered at 1000 °C and 1100 °C were at extreme high voltages and not be observed in the measuring range, although the E_b strongly decreased with increasing sintering temperature. Breakdown field E_b is related to the effective number of grain boundaries per length between the electrodes. As can be seen in Fig. 7 and Table 1, the decrease of E_b with increasing sintering temperature was attributed to the increase of average grain size only. In contrast, variation of E_b with the changes in Mn content originated for forming Schottky barriers discussed as follows.

In order to describe the E-J nonlinear behavior of the varistors, the barrier layer model based on the depletion layers within ZnO grains has been applied. In this model, the charges which are trapped in surface states at the intergranular layers dominate the two adjacent grains response to

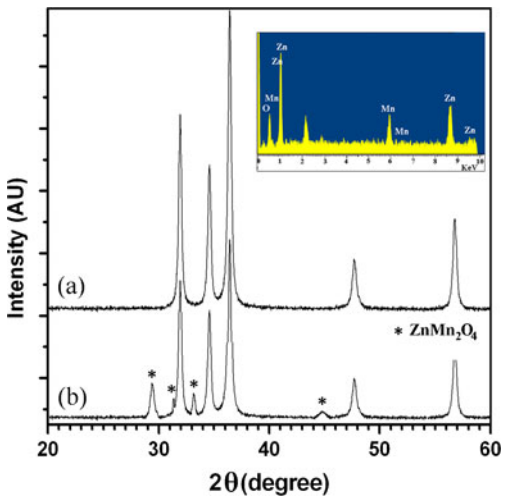

Fig. 5 XRD patterns of (*a*) ZnO and (*b*) 6 mol% Mn doped ceramics sintered at 1000 °C. The inset is the EDX from a particle formed at a triple point of 6 mol% Mn doped ceramic sintered at 1000 °C

low and high voltages. Levinson [3] states that the process associated to prebreakdown region is Schottky emission, corresponding to thermionic emission over the barrier layer. It may be concluded that Mn dose not play an important role in the ZnO conduction. However, as shown in the ohmic region of Fig. 6, Mn doping made ZnO a more resistive ceramic because of reducing the zinc interstitial concentration. The abnormal V-I behavior in 15 mol% Mn doped ceramic, sintered at 1000 °C can be due to the different oxidation degree of Mn atoms substituted instead of Zn^{+2} [26].

In the barrier layer model, because the electron traps on the surface of intergranular layer absorb electrons from adjacent grains, a potential barrier is formed. This trap formation can be affected by doping agents [27]. According to this model, the barrier can extend to the inside of grains. The thickness and height of this barrier, which also depends on sintering temperature and time duration, play the main role in nonlinear V-I characteristic of the specimens. Matsuoka [6] hints that in order to having sufficient trap sites and also barrier formation; the thickness of the depletion layer must exceed a critical value. Thus, it can be concluded that the thickness of depletion layer in the 15 mol% Mn doped specimen sintered at 1000 °C was not enough to show the V-I nonlinearity. However, with the increase in sintering temperatures, the depletion layer reached the reasonable condition and the varistor operation appeared.

The varistor behavior of pure ZnO originates for oxygen diffusion along grain boundaries. In this case, the amount of intrinsic acceptors (Zinc vacancies) could be more than intrinsic donors and the potential barrier is formed. Thus, the grain boundaries oxidation guarantees the varistor operation. Einzinger [28] asserts that the nonlinear V-I characteristic have been observed in undoped ZnO provided that the sintering process has been performed in a high-pressure oxygen atmosphere. This assumption agrees with the results obtained by Mantas et al. [16]. As shown in Fig. 6, we have prepared undoped ZnO ceramics exhibited varistor behavior. These undoped varistors were prepared with nanosized precursors and the average grain size was small. Because of the high surface to volume ratio in grains, the grain boundaries oxidation is possible when the specimens are slightly cooled down and sintering in the high-pressure oxygen atmosphere is not necessary.

Moreover, the dopants in ZnO structure can contribute to the grain boundaries oxidation process as discussed by Einzinger [29]. In this case, Mn atoms, which tend to be accumulated in the grain boundaries, bring about the migration of donors from bulk to boundaries in order to be annihilated during cooling process [30].

In the barrier layer model, a few important parameters affect the V-I characteristic of varistors including breakdown electric field E_b, barrier height φ_0, and the thickness

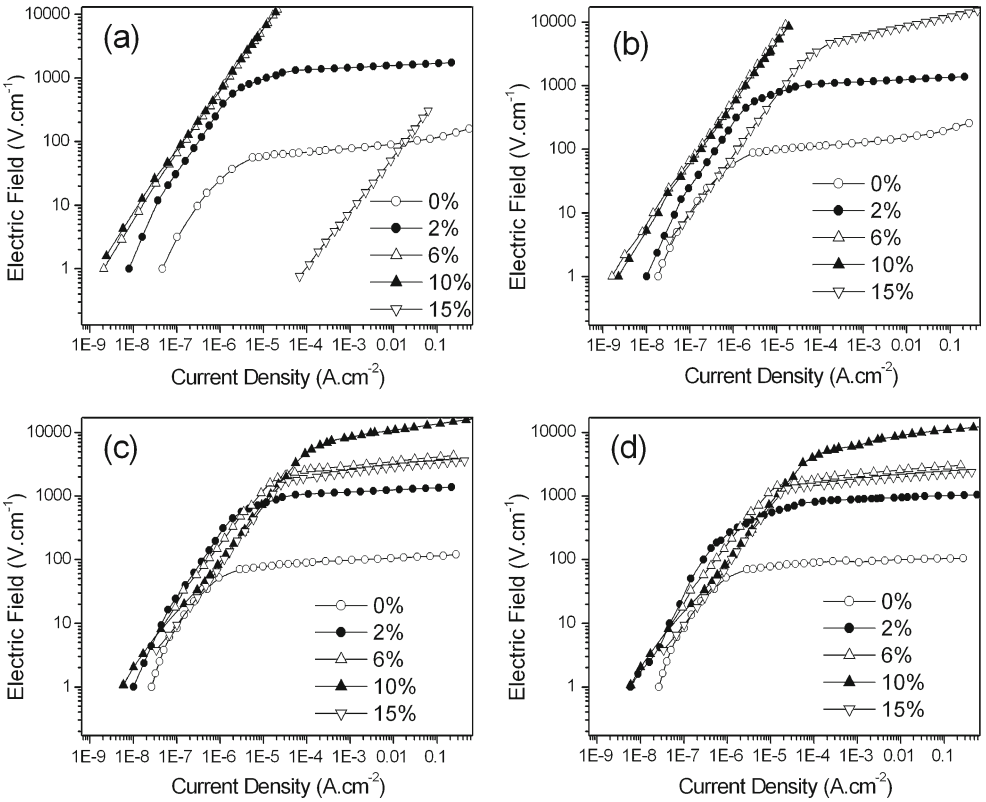

Fig. 6 Electric field – current density (E-J) characteristics of undoped ZnO and Mn doped ZnO varistors sintered at different temperatures (**a**) 1000 °C, (**b**) 1100 °C, (**c**) 1200 °C and (**d**) 1300 °C

Table 1 Nonlinear coefficient α, leakage current density J_l and breakdown electric field E_b of Mn doped ZnO varistors sintered at different temperatures

Mn Content (mol%)	Sintering Temperature (°C)	E_b (V/cm)	Nonlinear Coefficient	Leakage Current Density (μA/cm^2)
This work				
0.0	1000	89.12	17.25	10.47
0.0	1100	141.25	25.21	5.49
0.0	1200	100.00	22.13	2.45
0.0	1300	79.43	20.40	0.38
2.0	1000	1513.56	25.60	10.81
2.0	1100	1174.89	40.00	9.54
2.0	1200	1000.00	34.90	7.25
2.0	1300	891.25	30.30	6.51
6.0	1200	2951.21	9.50	12.59
6.0	1300	2238.72	25.35	8.85
10.0	1200	8709.63	8.80	24.65
10.0	1300	6309.57	14.28	15.20
15.0	1100	6456.54	6.70	25.54
15.0	1200	2324.23	8.90	18.25
15.0	1300	1778.28	12.20	15.22
Others [15]				
1.3	1000	9030	15.6	–
1.3	1100	480	17.5	–
1.3	1200	2120	7	–
1.3	1300	1183	6	–

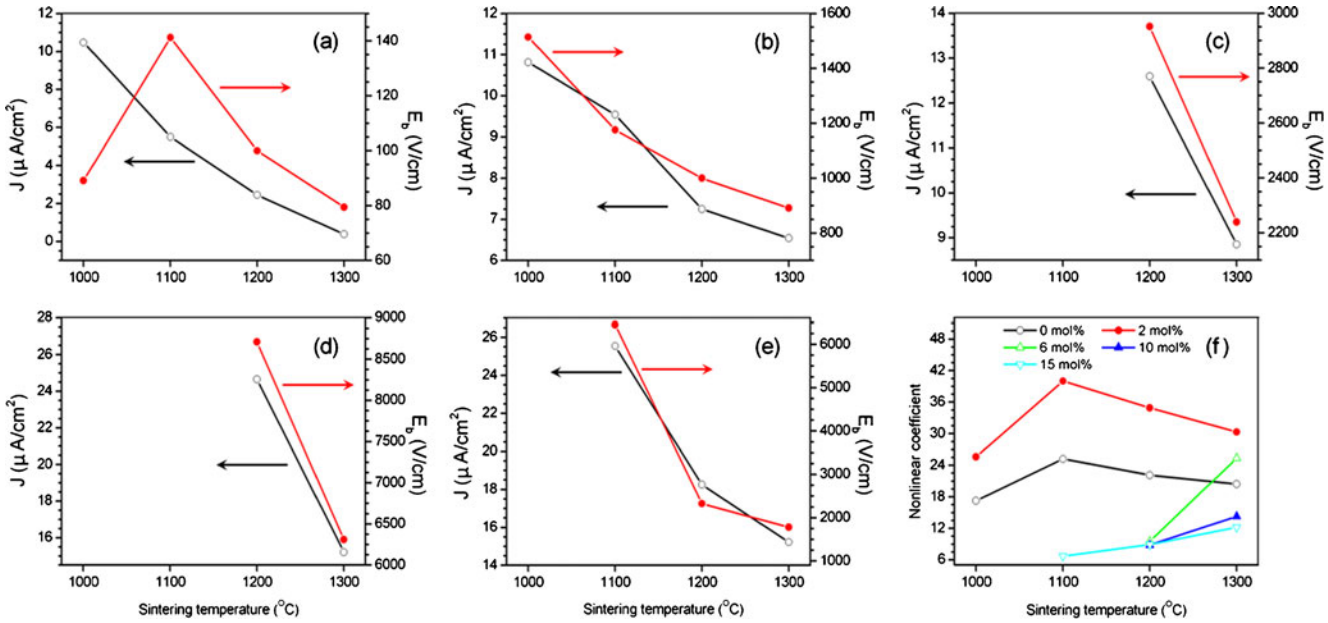

Fig. 7 Breakdown electric field E_b and leakage current density J_l as a function sintering temperature for ZnO varistors doped with various amount of Mn, (**a**) 0 mol%, (**b**) 2 mol%, (**c**) 6 mol%, (**d**) 10 mol% and (**e**) 15 mol%. (**f**) Nonlinear coefficient α as a function of sintering temperature and Mn content

of the depletion layer d. From Poisson's equation, the barrier height and depletion layer are [31]:

$$\varphi_0 = \frac{e^2 n_t^2}{8\varepsilon\varepsilon_0 n_0} \tag{1}$$

$$d \approx \left(\frac{\varepsilon\varphi_0}{n_0}\right)^{1/2} \tag{2}$$

where n_t is the density of the trapped charges, n_0 is the density of the carriers in the grains and ε is the dielectric constant of the ceramic. These relations show that the breakdown electric field depends on the density of the trap sites and their distribution in the surface of intergranular layer.

As can be seen in Table 1 and Fig. 7, the E_b increased as the doping level increased to 10 mol% and then decreased for further doping concentrations. Since Mn is rather a deep donor, the Mn atoms used as an additive in the ZnO based varistors have no effects on both conductivity and n_0 [16]. However, n_t and ε naturally vary with the change in the amount of Mn.

In Fig. 8, the measured dielectric constant ε as a function of frequency is plotted for the samples sintered at 1000 °C. The high dielectric constant reflects two phase nature of ZnO based varistors. ε decreased slightly, from 40 to 10^5 Hz, with a sharper drop evident in the range 10^5 to 10^6 Hz. Also, the results revealed that the value of ε obtained for Mn doped samples was much higher than that of for undoped ceramic. On the other hand, it is expected that the density of the trap states increases with the increase in Mn content in ZnO ceramic [16]. As a result, higher external voltages must be applied to fill these trap states. In this case, the barrier height in a ZnO grain varies slowly rather than adjacent grain until all traps are filled. As shown in Fig. 6, the breakdown electric field increased with the increase in the Mn content and kept rising for 10 mol% Mn doped sample. It can be concluded from relation (1) that the density of trap states plays more significant role in changing the barrier height and E_b than the dielectric constant.

From above discussion and Relation (2), the thickness of depletion layer increased with the increase of Mn content up to 10 mol%. On the other hand, the small values of E_b obtained for undoped varistor was probably attributed to two different factors. First, the results suggest that the Schottky barrier was not formed at all the grain boundaries. Second, relation (2) reveals that the small thickness of

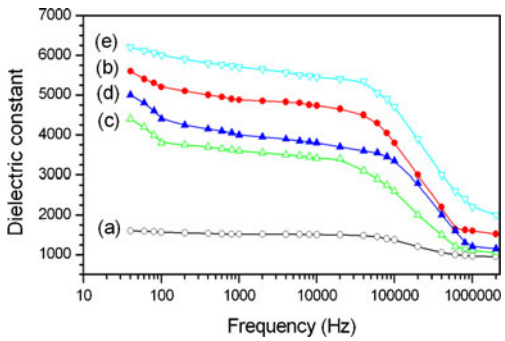

Fig. 8 Variation of room temperature dielectric constant of undoped and Mn doped ZnO varistor with frequency

depletion layer *d* of the undoped varistor caused the barrier height to decrease.

In this paper, the sintering temperature effects on the breakdown voltage have been also investigated. The changes in sintering process affect the microstructural properties such as grain size and homogeneity. The dependence of the breakdown field on dimensional properties has been discussed by Li et al. [19, 20]. Figure 6 indicates that the threshold electric field of heavily doped ceramics decreased with the increase of the sintering temperature. Larger grain size, heterogeneity in distribution of grain size and irregularities of the grains shape led to a decrease in density of the trap states, thereby bringing about the decrease of breakdown voltage [1, 25]. For example, the breakdown field measured for 10 mol% doped sample decreased from 8709 V/cm to 6309 V/cm, with 100 °C increase in the sintering temperature. This variation in breakdown field was attributed to reducing the number of grain boundaries per length unit. In this work, the optimum average grain size is found to be about 2 μm, which is much smaller than that of suggested for ZnO ceramics, fabricated from larger particles [32].

The most important feature in V-I characteristic in Fig. 6 is pointed out as breakdown region, which is related to existing intrinsic donors in interfaces. In this mechanism, the electrons can tunnel into the conduction band through the narrow potential barrier. In this case, the leakage current density J_l is defined as the amount of electrons which are passing over this barrier at grain boundaries. As given in Table 1, the leakage current densities of Mn doped specimens were higher than the pure ZnO ceramic which means that the electrons need lower energies to overcome the barrier. Also, the nonlinear coefficient α decreased with the Mn concentration further to 2 mol%. It was attributed to the increasing the insulator layer width. Levinson and Philipp [3] state that the so-called tunneling process preferably occurs through very thin insulator layers. Also, reduction in homogeneity of the microstructure due to high doping level was another reason for decreasing α in specimens with 6, 10 and 15 mol% doping levels.

Moreover, several studies have shown that controlling the type of orientation between ZnO and ZnO grain boundaries affect the electrical performance of the varistor. Özgür Özer et al. [33] suggested that the leakage current and Schottky barrier height along different directions were found to be changed due to an apparent crystallographic texture. Also, a strong correlation between the crystal orientation of ZnO grains and electrical degradation has been reported. Takada et al. [34] states that the mobility of oxygen ions decreases at grain boundary formed by the c-axis orientation of ZnO. But, all the samples sintered at 1000 °C were preferably crystallized in [101] orientation and no significant variation in relative intensity of diffraction peaks were observed with the changes in Mn content. From the above discussion, it is concluded that the variations in the electrical properties of the undoped and doped ceramics sintered at 1000 °C for 2 h were not attributed to ZnO grain orientation.

In an application of varistors, the two significant factors nonlinearity and its stability should be essentially considered. In order to protect the electronic equipments and power systems from surges, a high stability varistor is required. The varistors degrade because of gradually increasing leakage current I_l with stress time. Ultimately, they cause

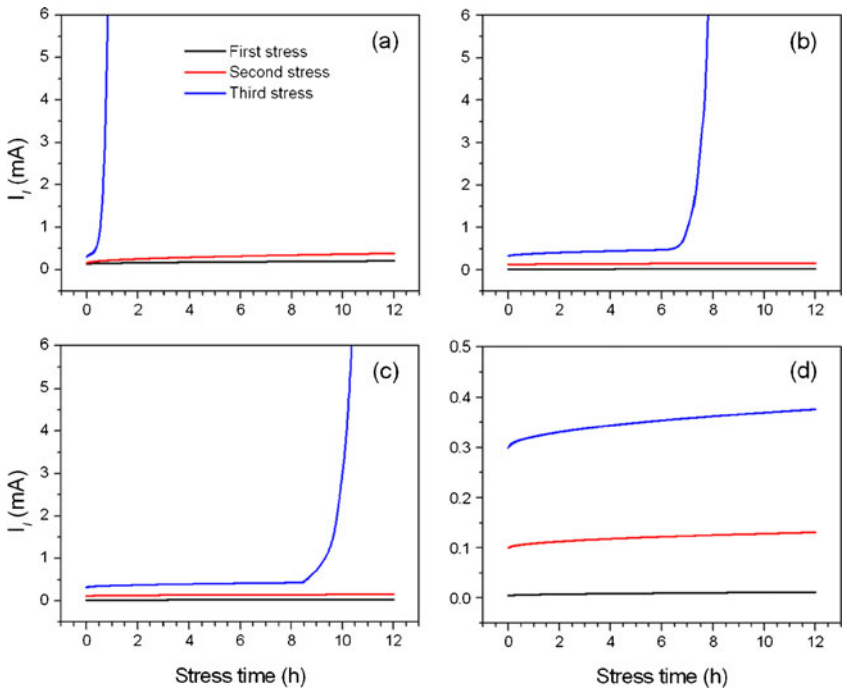

Fig. 9 The leakage current I_l during various DC accelerated aging stress of undoped ZnO varistors sintered at different temperatures, (**a**) 1000 °C, (**b**) 1100 °C, (**c**) 1200 °C and (**d**) 1300 °C under first, second and third stresses

the thermal runaway and loss of varistor behavior. The rate of degradation can be strongly affected by small changes in the chemical composition and fabrication processing, as well as by heat treatments. Also, the degradation process affects mainly the leakage and prebreakdown region and not the V-I characteristic above the breakdown voltage. Therefore, electrical stability is an important property of the varistor, perhaps the most striking. Figure 9 shows the leakage current I_l during various stresses subjected to the undoped varistors sintered at temperature 1000 °C to 1300 °C. Generally, even if the nonlinear V-I characteristic is observed in undoped ZnO varistors, it is unstable and not reproducible. However, all the undoped ceramics is stable under first and second stresses. But, the undoped ZnO varistor sintered at 1000 °C exhibited the thermal runaway under the third stress within a short time. On the other hand, the undoped ceramic sintered at 1300 °C showed much higher stability, compared with the undoped samples sintered at lower temperatures. The stability of varistors seems to be affected by density and leakage current. This high stability of ZnO varistor sintered at 1300 °C may be attributed to the high density and the low leakage current. From above discussion, it is suggested that undoped ZnO varistors with high density exhibits much higher stability and one way of achieving higher densities is fabricating the ceramics from nanosized precursors.

4 Conclusions

In this work, Mn doped ZnO varistors were manufactured from nanosized precursors at different sintering temperatures and their properties were investigated. SEM images clearly showed that the microstructural homogeneity of the specimens was improved compared with those of conventional mixed oxide technique. E-J characteristics of the samples indicated that the grain boundaries oxidation process, which guarantees the varistor operation, was successfully turned out. The barrier layer model was used to explain the effect of doping and sintering temperature on the breakdown field. The origin of the varistor operation is attributed to creating more trap states with the increase of Mn content and decreasing the barrier height with increasing sintering temperature. The best nonlinearity was observed in the sample was with 2 mol% doping level, sintered at 1100 °C. In addition to chemical composition of a varistor, nonlinear V-I characteristic depends on the microstructure properties of the ceramics, such as grain size, intergranular layer thickness and porosity. The homogeneity, small size of grains and narrow distribution of barrier heights contributed to the large nonlinearity of the components and better stability.

References

1. L.M. Levinson, H.R. Philipp, Am. Ceram. Soc. Bull. **65**, 639 (1986)
2. D.R. Clarke, J. Am. Ceram. Soc. **82**, 485 (1999)
3. L.M. Levinson, H.R. Philipp, J. Appl. Phys. **46**, 1332 (1975)
4. P.L. Hower, T.K. Gupta, J. Appl. Phys. **50**, 4847 (1979)
5. G.D. Mahan, L.M. Levinson, H.R. Philipp, J. Appl. Phys. **50**, 2799 (1979)
6. M. Matsuoka, Jpn. J. Appl. Phys. **10**, 736 (1971)
7. C.H. Nahm, Solid State Commun. **149**, 795 (2009)
8. C.-H. Kim, J.-H. Kim, J. Europ. Ceram. Soc. **24**, 2537 (2004)
9. M. Houabes, R. Metz, Ceram. Int. **33**, 1191 (2007)
10. H.I. Oh, J.H. Kim, J. Electroceram. **17**, 1083 (2006)
11. D. Xu, L. Shi, Z. Wu, Q. Zhong, X. Wu, J. Europ. Ceram. Soc. **29**, 1789 (2009)
12. J. Fan, R. Freer, J. Appl. Phys. **77**, 4795 (1995)
13. A.B. Alles, V.L. Burdick, J. Appl. Phys. **70**, 6883 (1991)
14. C.-W. Nahm, Solid State Commun. **141**, 685 (2007)
15. Y.W. Hong, J.H. Kim, Ceram. Int. **30**, 1301 (2004)
16. J. Han, A.M.R. Senos, P.Q. Mantas, J. Europ. Ceram. Soc. **22**, 1653 (2002)
17. H.I. Oh, J.H. Kim, J. Electroceram. **17**, 1083 (2006)
18. R.C. Buchanan, *Ceramic materials for electronics* (Marcel Dekker Inc, NewYork, 1991)
19. S. Li, J. Li, F. Liu, M.A. Alim, G. Chen, J. Phys. D: Appl. Phys. **35**, 1884 (2002)
20. S. Li, J. Li, M.A. Lim, J. Electroceram. **11**, 119 (2003)
21. L.T. Harry, J. Electroceram. **4**, 33 (1999)
22. C.-W. Nan, D.R. Clarck, J. Am. Ceram. Soc. **79**, 3185 (1996)
23. M.S. Wang, S.H. Oh, C.B. Park, IEEE Nanotechnology materials and devices conference, S. Korea (2006)
24. J. Zhang, S. Cao, R. Zhang, L. Yu, C. Jing, Current Appl. Phys. **5**, 381 (2005)
25. L. Cong, F. Zhuowei, X. Zheng, X. Yewen, J. Electroceram. **21**, 423 (2008)
26. M. Ebrahimizadeh Abrishami, S.M. Hosseini, E. Attaran Kakhki, A. Kompany, M. Ghasemifard, Int. J. Nanosci. **9**, 19 (2010)
27. C. Leach, K.D. Vernon-Parrym, N.K. Ali, J. Electroceram. **25**, 188 (2010)
28. R. Einzinger, Ann. Rev. Mater. Sci. **17**, 299 (1987)
29. R. Einzinger, Mat. Res. Soc. Symp. **343** (1982)
30. B. Straumal, B. Baretzky, A. Mazilkin, S. Protasova, A. Myatiev, P. Straumal, J. Europ. Ceram. Soc. **29**, 1963 (2009)
31. J. Shi, Q. Cao, Y. Wei, Y. Huang, Mater. Sci. Eng. B **99**, 344 (2003)
32. O.A. Fregoso, Rev. Mex. Fis. **40**, 771 (1994)
33. İ. Özgür Özer, E. Suvaci, S. Bernik, Acta Mater. **58**, 4126 (2010)
34. M. Takada, H. Yoshino, S. Yoshkado, Key Eng. Mater. **350**, 213 (2007)